Chapter 5

A Three-dimensional of Coastline Deformation using the Sorting Reliability Algorithm of ENVISAT Interferometric Synthetic Aperture Radar

Maged Marghany

Additional information is available at the end of the chapter

http://dx.doi.org/10.5772/58571

1. Introduction

At present, because of sea-level rise, and climate change (such as an increase in storm surges, hurricanes, etc.) there is a worldwide increase in coastal erosion, usually apparent in the progressive retreat of backshore cliffs, dunes, spits, and the concomitant landward displacement of the shoreline [10, 13, 21]. In this regard, coastal erosion requires standard procedures for monitoring, modelling, and mapping [12, 22].

In the last two decades, scientists have developed a powerful technique to measure the millimeter-scale of the Earth 's surface deformation by comparing complex synthetic aperture radar (SAR) data that were acquired a few days or a few years apart. This technique is known as interferometric synthetic aperture radar (InSAR). Accurate Earth 's surface deformation or digital elevation maps can be produced by implementing the single look complex synthetic aperture radar (SAR) images that are received by two or more separate antennas. The phase image is produced by multiplying the complex SAR image by the coregistered complex conjugate pixels of the other SAR data. Image coregistration, InSAR interferometric phase estimation (or noise filtering) and interferometric phase unwrapping [3, 4, 5, 6, 32, 37, 41] are three key processing procedures of InSAR.

Therefore, advance application of remote sensing technology such as interferometric synthetic aperture radar (InSAR) for coastal geomorphology study is in a preliminary stage. InSAR has shown that it can provide DEMs with 1-10 cm accuracy, which can be improved to millimeter level by Differential synthetic aperture radar Interferometry (DInSAR) [1, 3, 5, 8, 22].

Therefore, InSAR techniques are proven to provide precisely digital elevation model map (DEMs). In this context, mapping purposes, geomorphological studies based on aspect maps and slops are acquired highly accurate DEMs products. In this regard, sub-centimeter target displacements can be detected using DInSAR along the sensor-target direction [5, 10, 17]. In comparison with other conventional techniques such as levelling, and GPS, DInSAR provides valuable information about target displacement, over large areas, at a relatively low cost [2, 6]. In fact, conventional methods are time consuming and they are required some control points [1, 9]. DInSAR has many other applications as well, such as monitoring geophysical natural hazards, for instance, earthquakes, volcanoes and landslides, also in engineering, in particular recording of subsidence and structural stability. Overtime-spans of days to years, InSAR can detect the centimeter-scale of deformation changes [4]. Furthermore, the precision of DEMs from the InSAR technique is quite high, compared to conventional remote sensing methods. In many countries, the 90 m SRTM data, or the 30 m. DEM data from ASTER are the main sources of DEMs [15, 17].

1.1. Problems in interferometric techniques

It is well known that the performance of the interferometric phase estimation suffers seriously from poor image coregistration. Interferogram filtering algorithms such as adaptive contoured window, pivoting mean filtering, pivoting median filtering, and adaptive phase noise filtering [15] are the main methods for the conventional InSAR interferometric phase estimation. These filtering algorithms, nevertheless cannot retrieve the accurate terrain interferometric phases from a poor interferogram because of coregisteration errors and high decorrelation. Indeed, the interferometric phases are random in nature with their variances being inversely proportional to the correlation coefficients between the corresponding pixel pairs of the two coregistered SAR data. Therefore, the terrain interferometric phases should be estimated statistically [34-41].

It is well known that the accuracy of the image coregistertion is a serious issue for accuracy interferometric phase unwrapping. Therefore, the conventional phases unwrapping algorithms, such as the branch-cut method, region-growing method and the least-square one, which are required accurate image coregistration to be about 1/10 to 1/100 resolution cell size (i.e., SAR pixel). Nevertheless, the optained InSAR phase unwrapping will be extremely noises if InSAR data coregisteration is decorrelated. In this regard, the accurate InSAR data coregisteration is a hard task with low coherence data which is extremely change dynamically [41]. In this context, Hai L and Renbiao [41] stated that the interferometric phase estimation method based on subspace projection can provide an accurate estimation of the terrain interferometric Phase (interferogram) even if the coregistration error reaches one pixel.

Incidentally, the phase difference of the two SAR data is processed to acquire height and deformation of the Earth's surface. Therefore, scientists have agreed that the accurate results of InSAR are required standard criteria for data acquisitions. According to Hanssen [3], short temporal baseline, appropriate spatial baseline, good weather conditions and ascending and descending SAR data are regular criteria to reduce decorrelation and noise and produce a reliable DEM.

Nonetheless, alternative SAR datasets must obtain at high latitudes or in zones of run-down coverage [6, 13]. The baseline decorrelation and temporal decorrelation, nevertheless, make InSAR measurements unrealistic [8, 9, 10, 11]. Incidentally, Gens [12] stated the length of the baseline designates the sensitivity to height changes and sum of baseline decorrelation. Additional, Gens [12] reported the time difference for two data acquisitions is a second source of decoration. Indeed, the time differences while compare data sets with a similar baseline length acquired one and 35 days apart suggests only the temporal component of the decorrelation. Therefore, the loss of coherence in the same repeat cycle in data acquisition is most likely because of baseline decorrelation. According to Roa et al. [7], uncertainties could arise in DEM because of limitation InSAR repeat passes. In addition, the interaction of the radar signal with troposphere can also induce decorrelation. This is explained in several studies [3, 8, 15].

Commonly, the propagation of the waves through the atmosphere can be a source of error exist in most interferogram productions. When the SAR signal propagated through a vacuum it should theoretically be subjected to some decent accuracy of timing and cause phase delay [3, 21]. A constant phase difference between the two images caused by the horizontally homogeneous atmosphere was over the length scale of an interferogram and vertically over that of the topography. The atmosphere, however, is laterally heterogeneous on length scales both larger and smaller than typical deformation signals [9, 23]. In other cases the atmospheric phase delay, however, is caused by vertical inhomogeneity at low altitudes and this may result in fringes appearing to correspond with the topography [24]. Under this circumstance, this spurious signal can appear entirely isolated from the surface features of the image, since the phase difference is measured other points in the interferogram, would not contribute to the signal [3, 17]. This can reduce seriously the low signal-to-noise ratio (SNR) which restricted to perform phase unwrapping. Accordingly, the phases of weak signals are not reliable. According to Yang et al., [11], the correlation map can be used to measure the intensity of the noise in some sense. It may be overrated because of an inadequate number of samples allied with a small window [9]. Weights are initiated to the correlation coefficients according to the amplitudes of the complex signals to estimate accurate reliability [11, 18].

According to Pepe [40] DinSAR has recently been applied with success to investigate the temporal evolution of the detected deformation phenomena through the generation of displacement time-series. In this case, the analysis is based on the computation of deformation time-series via the inversion of a properly chosen set of interferograms, produced from a sequence of temporally-separated SAR acquisitions relevant to the investigated area. In this context, two main categories of advanced DInSAR techniques for deformation time-series generation have been proposed in literature, often referred to as Persistent Scatterers (PS); and Small Baseline (SB) techniques, respectively. The PS algorithms select all the interferometric data pairs with reference to a single common master image, without any constraint on the temporal and spatial separation (baseline) among the orbits. In this case, the analysis is carried out on the full resolution spatial scale, and is focused on the pixels

containing a single dominant scatterer thus ensuring very limited temporal and spatial decorrelation phenomena.

1.2. Hypotheses and objectives

In this paper, we address the question of utilization three-dimensional phase unwrapping algorithm to estimate rate changes of shoreline deformation. In fact, there are several factors could impact the accuracy of DEMs was derived from phase unwrapping [21]. These factors are involved radar shadow, layover, multi-path effects and image misregistration, and finally the signal-to –noise ratio (SNR) [11]. This demonstrated with ENVISAT ASAR data. The main contribution of this study is to implement three three-dimensional phase unwrapping algorithm with InSAR technique. Three hypotheses examined are: (i) three-dimensional phase unwrapping algorithm can be used as filtering technique to reduce noise in phase unwrapping; (ii) 3-D shoreline reconstruction can be produced using satisfactory phase unwrapping by involving the three-dimensional phase unwrapping algorithm; and (iii) high accuracy of deformation rate can be estimated by using the new technique.

2. Study area

The study area is located along the coast of Johor in the southern eastern part of Peninsular Malaysia. The area is approximately 20 km of Johor (Figure 1), located in the South China Sea, between 1° 57′ N to 2° 15′ N and 103° 51′ E to 104° 15′ E. This coastline is exhibited a variety of geomorphologies that includes sandy beaches, rocky headlands which is broken by small river mouths. In addition, the coastline has hilly terrain with steep slopes and deep narrow valleys. Further, the coastline is bordered with varying widths of alluvial plains. Further, sand materials make up the entire of the eastern Johor shoreline. Consistent with Marghany [42], this area lies in an equatorial region dominated by two seasonal monsoons and two inter monsoon periods. The southwest monsoon lasts from May to September while the northeast monsoon lasts from November to March. The inter monsoon periods involve April which is between end of northeast monsoon and beginning of the southwest monsoon periods. Further, the second inter monsoon period is October which is between the end of the southwest monsoon and the beginning of northeast monsoon periods. The monsoon winds affect the direction and magnitude of the waves. Further, Marghany [14, 42] stated that strong waves are prevalent during the northeast monsoon when the prevailing wave direction is from the north (November to March), while during the southwest monsoon (May to September), the wave directions are propagated from the south. According to Marghany [14] the maximum wave height during the northeast monsoon season is 4 m. The minimum wave height is found during the southwest monsoon which is less than 1 m [18].

http://dx.doi.org/10.5772/58571

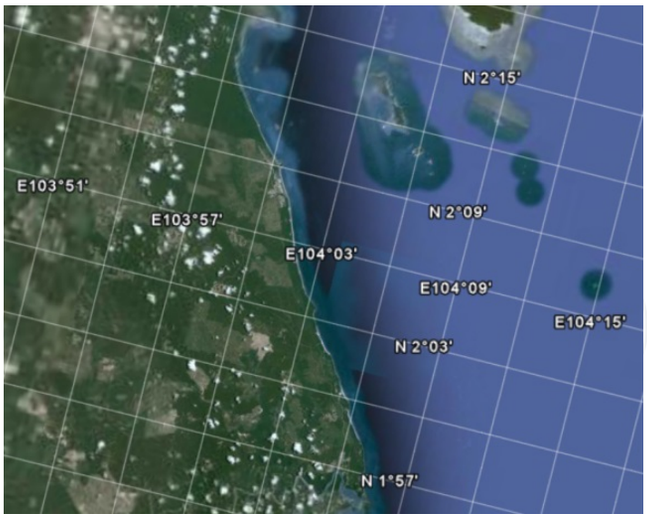

Figure 1. Location of study area

3. InSAR data processing

Two methods are involved to perform InSAR from ENVISAT ASAR SAR data (i) conventional InSAR procedures; and (ii) three-dimensional phase unwrapping algorithm i.e. three-dimensional sorting reliabilities algorithm (3D-SRA) [25, 42]

3.1. Conventional InSAR method

According, Zebker et al., [4], two complex SAR data are required to achieve InSAR procedures. These complex SAR data have a real (cosine) and an imaginary (sine) components. Then real and an imaginary components are combined as vectors to acquire information of phase and intensity of the SAR signal [10]. In Marghany [26], the surface displacement can estimate using the acquisition times of two SAR data S_1 and S_2. The component of surface displacement, thus, in the radar-look direction (Figure 2), contributes to the further interferometric phase (φ) as [9]

$$\phi = \frac{4\pi(\Delta R)}{\lambda} = \frac{4\pi(B_h \sin\theta - B_v \cos\theta)}{\lambda} \quad (1)$$

where ΔR is the slant range difference from satellite to target respectively at different time, θ is the look angle (19.2-26.7°), (Table 1) and λ is the ENVISAT ASAR wavelength Single Look Complex (SLC) which is about 5.6 cm for C-band. Therefore, B_h, B_v are horizontal and vertical baseline components[19].

According to Lee [9], for the surface displacement measurement, the zero-baseline InSAR configuration is the ideal as $\Delta R = 0$, so that

$$\phi = \phi_d = \frac{4\pi}{\lambda}\zeta \tag{2}$$

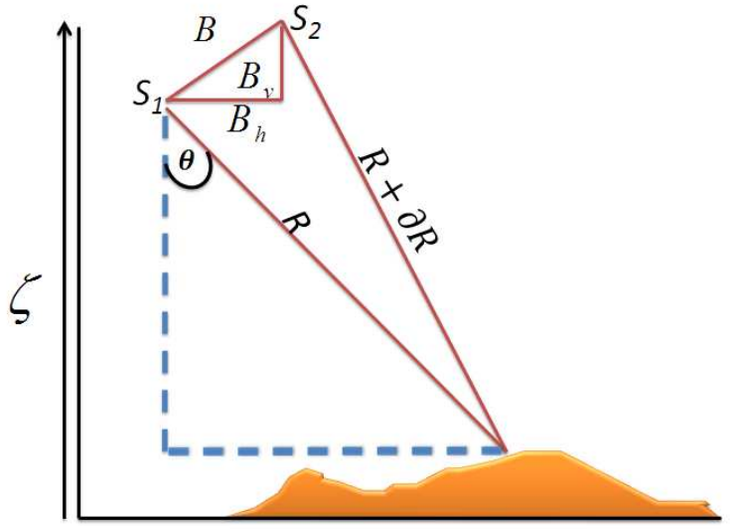

Figure 2. InSAR Geometry.

Parameters	Values
Radar Wavelength (cm)	5.6
Ground Resolution	30
Swath Width (km)	105
Incident Angle (°)	19.2-26.7
Polarization	HH/VV

Table 1. ENVISAT ASAR characteristics were used in this study [19, 42]

In actual fact, zero-baseline, repeat-pass InSAR configuration is hardly achievable for either spaceborne or airborne SAR. Therefore, a method to remove the topographic phase as well as the system geometric phase in a non-zero baseline interferogram is needed. If the interferometric phase from the InSAR geometry and topography can strip off from the interferogram, the remnant phase would be the phase from block surface movement, providing the surface maintains high coherence [5]. Then, the phase difference $\Delta\phi$ between the two ENVISAT ASAR data positions and the pixel of target of terrain point is given by

$$\Delta\zeta = \frac{\lambda R \sin\theta}{4\pi B}\Delta\phi \tag{3}$$

http://dx.doi.org/10.5772/58571

Equation 3 is a function of normal base line *B*, and the range *R*. In addition, equation 3 can provide information about the heights and phase differences estimations. In fact, the estimated height of each pixel of ENVISAT ASAR data is an important task to generate a raster form of the DEM.

3.2. DEM reconstruction using a three-dimensional Sorting Reliabilities Algorithm (3D-SRA)

Marghany [42] has adapted the algorithm introduced by Hussein et al., [25] for three-dimensional phase unwrapping the algorithm that is called a three-dimensional sorting reliability algorithm (3D-SRA). The quality of each edge of phase unwrapping is a function of the connection of two voxels in 3-D Cartesian axis e.g.,*x*,y, *z*. Starting, to carry out the unwrapping path from high quality voxels to bad quality voxels [25]. In addition, following a discreet path, the 3D-SRA algorithm unwraps the phase volume, which is significant to determine the 3-D volume change rate of shoreline. In this regard, the voxels connects the highest reliable edges that are unwrapped first with border surfaces. Consistent with Hussien et al., [26], the reliability value of an edge that connects a border voxel with another voxel in the phase volume is set to zero.

Let E_x, E_y, and N are the horizontal, vertical, and normal second differences, respectively which are given by

$$E_x(i,j,k) = \gamma[\phi(i-1,j,k) - \phi(i,j,k)] - \gamma[\phi(i,j,k) - \phi(i+1,j,k)], \tag{4}$$

$$E_y(i,j,k) = \gamma[\phi(i,j-1,k) - \phi(i,j,k)] - \gamma[\phi(i,j,k) - \phi(i,j+1,k)], \tag{5}$$

$$N(i,j,k) = \gamma[\phi(i,j,k-1) - \phi(i,j,k)] - \gamma[\phi(i,j,k) - \phi(i,J,k+1)], \tag{6}$$

where *i,j,k* are the neighbors' indices of the voxel in 3 x 3 x 3 cube, and γ defines a wrapping operator that wraps all values of its argument in the range $[-\pi, \pi]$. This can be done by adding or subtracting an integer number of 2 π rad to its argument [26]. γ can calculate from the wrapped-phase gradients in the *x*, *y*, and *z* directions as follows [25,26]

$$\gamma(i,j,k) = \frac{\partial \phi_{i,j,k}{}^{x}}{[\phi_{i+1,j,k} - \phi_{i,j,k}]}, \tag{7}$$

$$\gamma(i,j,k) = \frac{\partial \phi_{i,j,k}{}^{y}}{[\phi_{i,j+1,k} - \phi_{i,j,k}]}, \tag{8}$$

$$\gamma(i,j,k) = \frac{\partial \phi_{i,j,k}{}^{z}}{[\phi_{i,j,k+1} - \phi_{i,j,k}]}, \tag{9}$$

Equations 7 to 9 are represented 3-D array of the wrapped-phase gradients $\partial\phi^{x}$, $\partial\phi^{y}$, $\partial\phi^{z}$ and each has the same dimensions as the wrapped-phase volume. In addition, the maximum phase gradient measures the magnitude of the largest phase gradient that is, partial derivative or wrapped the phase difference in a *v*v*v* volumes [25]. Using the sum of equations 4 to 6, the second difference quality map *Q* can be obtained [26]

$$Q_{i,j,k} = \sqrt{E_x{}^2(i,j,k) + E_y{}^2(i,j,k) + N^2(i,j,k} \tag{10}$$

The unwrapping path is performed based on equation 10 where entirely the edges are stored in a 3D array and sorted with their edge quality values [26]. Further, unwrapping a voxel or a group of voxels concerning another group may require the addition or subtraction of multiples of 2 π [25]. In addition, the badness of each voxel in a *v*v*v* volume is determined by

$$b = \max\begin{Bmatrix} \max\left\{\left|\partial \phi_{i,j,k}{}^{x}\right|\right\} \\ \max\left\{\left|\partial \phi_{i,j,k}{}^{y}\right|\right\} \\ \max\left\{\left|\partial \phi_{i,j,k}{}^{z}\right|\right\} \end{Bmatrix} \tag{11}$$

b is the badness of voxel *(m,n,l),* which is given by

$$\begin{aligned} b = v^{-3} * [&\sqrt{\sum(\partial \phi_{i,j,k}{}^{x} + \overline{\partial \phi_{i,j,k}{}^{x}})^2} \\ &+\sqrt{\sum(\partial \phi_{i,j,k}{}^{y} + \overline{\partial \phi_{i,j,k}{}^{y}})^2} \\ &+\sqrt{\sum(\partial \phi_{i,j,k}{}^{z} + \overline{\partial \phi_{i,j,k}{}^{z}})^2}] \end{aligned} \tag{12}$$

where $\overline{\partial \phi_{i,j,k}{}^{x,y,z}}$ are the mean value of wrapped phase gradients in *x,y,z* directions, respectively through a *v*v*v* volume that are centered at at that voxel [25].

3.3. Ground survey

At the rear of Marghany [14], the GPS survey used to: (i) to record the exact geographical position of the shoreline; (ii) to determine the cross-sections of shoreline slopes; (iii) to corroborate the reliability of InSAR data co-registered; and finally, (iv) to create a reference network for future surveys. The geometric location of the GPS survey was obtained by using the new satellite geodetic network, IGM95. After a careful analysis of the places and to identify the reference vertexes, we thickened the network around such vertexes to perform the measurements for the cross sections (transect perpendicular to the coastline). The GPS data collected within 50 sample points scattered along 10000 m coastline. The interval distance of 2000 m between each sample location is considered. In every sample location, Rec-Alta (Recording Electronic Tachometer) was used to acquire the coastline elevation profile. The ground truth data were acquired on January 25 2011 during satellite passes.

4. Results and discussion

In this study, ENVISAT ASAR satellite data were used to investigate shoreline change using three-dimensional sorting reliability algorithm. InSAR methods are implemented on ENVISAT ASAR data sets of 5 March 2003 (SLC-1), 28 December 2010 (SLC-2) and January 25, 2011, (SLC-3) of Wide Swath Mode (WSM) (Figure 3). They are acquired from ascending (Track: 226, orbit: 5290), descending (Track:490, Orbit: 6055) and descending (Track 420,Orbit 4655), respectively. These data are in C band with VV polarization.

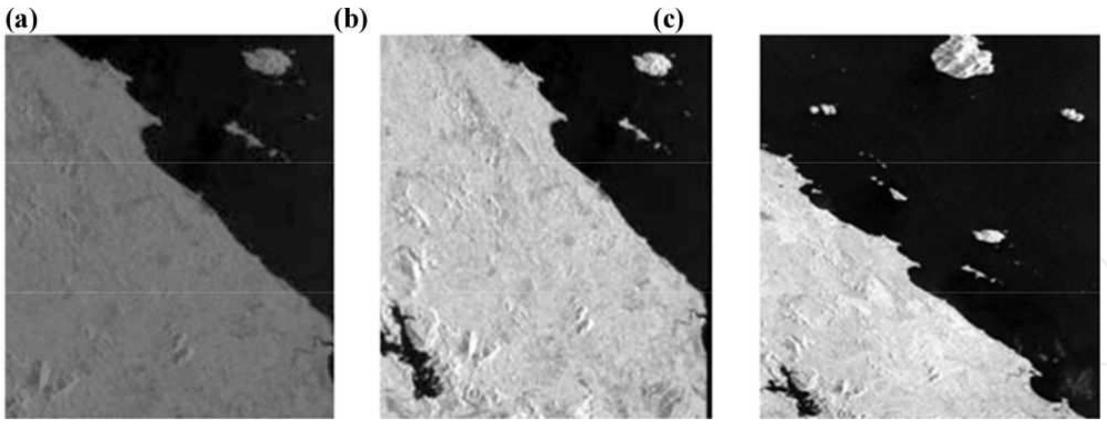

Figure 3. ENVISAT ASAR data used in this study (a) 5 March 2003; (b) 28 April 2003; and (c) January 25 2011

These data are C-band and had the lower signal-to-noise ratio owing to their VV polarization with a wavelength range of 3.7 to 7.5 cm and a frequency of 5.331 GHz. ASAR can achieve a spatial resolution generally around 30 m. The ASAR is intended for applications which require the spatial resolution of spatial resolution of 150 m. This means that it is not effective at imaging areas in depth, unlike stripmap SAR. The azimuth resolution is 4 m, and range resolution ranges between 8 m.

Figure 4 presents the reference DEM which has been generated from topographical 1:50000, and in situ measurements, respectively while Figure 4c shows the ENVISAT coherence data. It is clear that the maximum elevation of 50 m found inland. The maximum elevation of 10 m is shown along the coastline. The high coherence rates are existed in urban zone and along infrastructures with 0.9 while low coherence of 0.2 is found in a vegetation zone along the coastline. Since three ASAR data acquired in the wet northeast monsoon period, there has been an impact of wet sand on a radar signal penetration which causing weak penetration of radar signal because of the dielectric. Indeed, the total topographic decorrelation effects along the radar-facing slopes are dominant and highlighted as lowest coherence value of 0.2. According to Marghany [27] the micro-scale movement of the sand particles driven by the coastal hydrodynamic, and wind speed of 12 m/s during the northeast monsoon period [30] could change the distribution of scatters resulting in rapid temporal decorrelation which has contributed to lowest coherence along coastline. This result agreed with Marghany [27, 31].

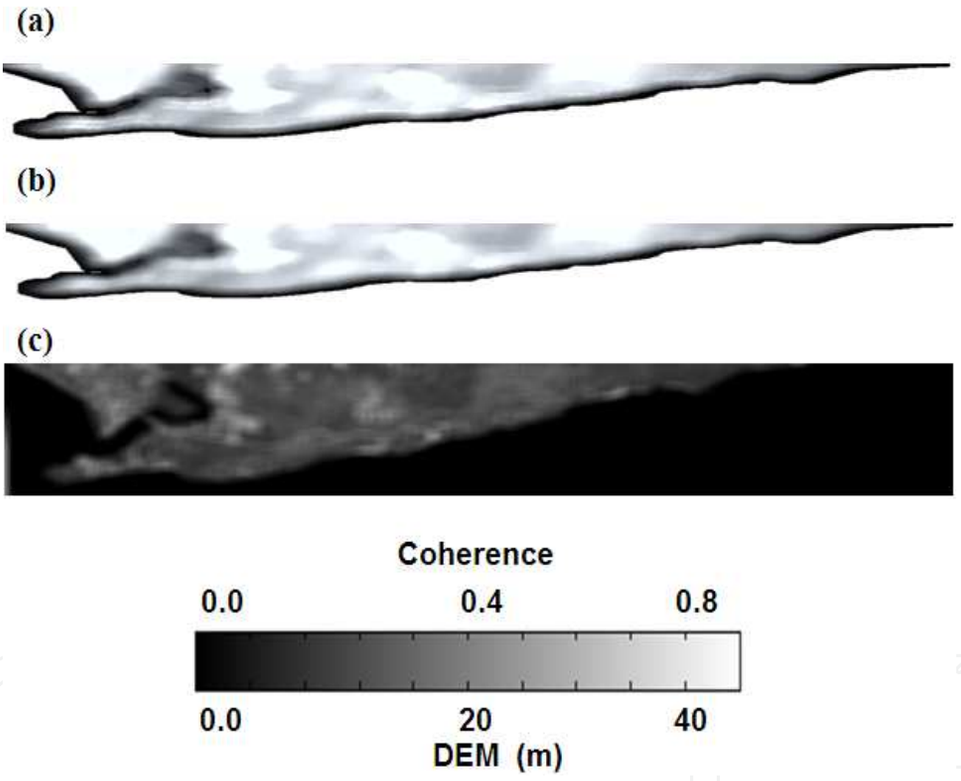

Figure 4. DEM generated from (a) topographic map; (b) in situ measurements; and (c) coherence ENVISAT ASAR

Cleary, there is huge differences between InSAR DEM and DEM generated from in situ measurements with 9 m differences while in situ measurements are concurred with DEM produced from topographic map within 1.3 m differences (Figure 5). This is because the impact of decorrelation. This result confirms the work done by Marghany [27, 29]. The overall scene is highly incoherent (Figure 4) which extremely effected the accuracy of InSAR DEM. This decorrelation caused a poor detection of InSAR DEM which induce large ambiguities because of poor coherence and scattering phenomenology. Indeed, the signatures of the interferometric

http://dx.doi.org/10.5772/58571

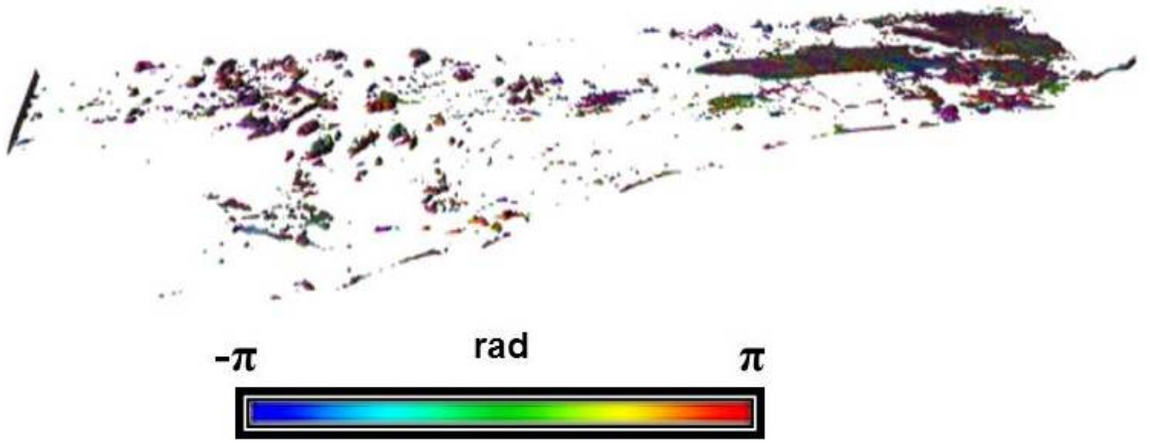

Figure 6. Interferogram generated from InSAR data

coherence and phase of vegetation are extremely impacted by temporal decorrelation in ASAR c-band data.

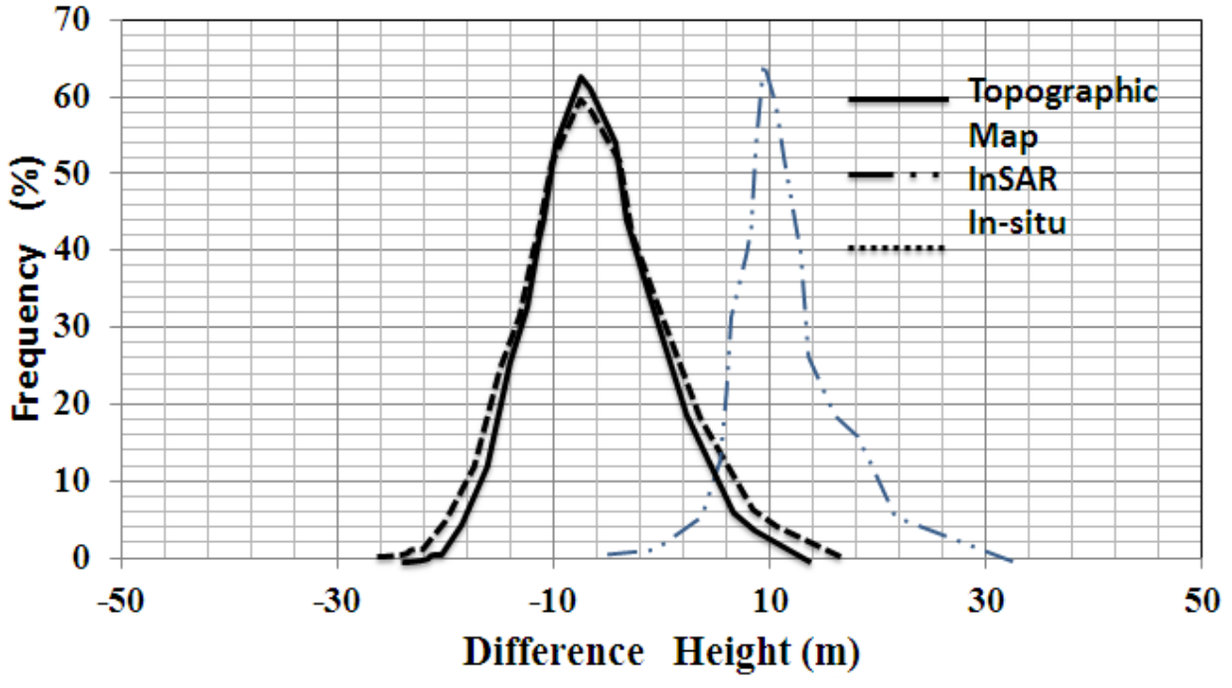

Figure 5. Height differences between DEM generated from InSAR, topographic map and in situ measurements.

According to Marghany [27], the ground ambiguity and ideal assumption that volume-only coherence can be acquired in at least one polarization. This assumption may fail when vegetation is thick, dense, or the penetration of an electromagnetic wave is weak. This agrees with the studies of Lee [9]; Marghany [14]; and Marghany [28, 29]. This can be seen clearly in InSAR interfeogram has been made from ASAR data (Figure 6).

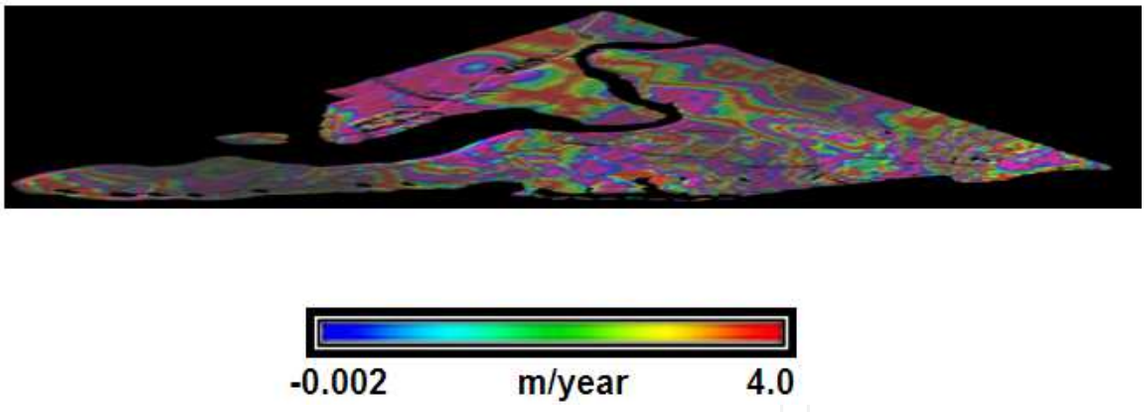

Figure 7. Fringe interferometry generated by a the three-dimensional sorting reliabilities algorithm

Figure 7 shows the interferogram created using three-dimensional sorting reliabilities algorithm 3-DSR. The full color cycle represents a phase cycle, covering the range between $-\pi$ to π. In this context, the phase difference given module 2 π; is color encoded in the fringes. Seemingly, the color bands change in the reverse order, indicating that the center has a critical coastline erosion of-3.5 m/year. This shift corresponds to 2 of coastal deformation over the distance of 10000 m.

Table 2 shows the statistical comparison between the simulated DEM from the InSAR, real ground measurements and with using three-dimensional sorting reliabilities algorithm. This table represents the bias (averages mean the standard error, 90 and 95% confidence intervals, respectively. Evidently, the InSAR using three-dimensional sorting reliabilities algorithm has a bias of-0.08 m, lower than ground measurements and the InSAR method. Therefore, a three-dimensional sorting reliabilities algorithm has a standard error of mean of ± 0.05 m, lower than ground measurements and the InSAR method. Overall performances of InSAR method using a three-dimensional sorting reliabilities algorithm is better than the conventional InSAR technique which is validated by a lower range of error (0.06±0.32 m) with 90% confidence intervals.

Statistical parameters	**InSAR techniques**			
	InSAR		**Three-dimensional sorting reliabilities algorithm**	
Bias	3.3		-0.08	
Standard error of the mean	2.2		0.05	
90% (90% confidence interval	Lower	Upper	Lower	Upper
	2.3	3.8	0.06	0.24
	1.3	3.2	0.04	0.32

Table 2. Statistical Comparison between InSAR and InSAR-three-dimensional sorting reliabilities algorithm

http://dx.doi.org/10.5772/58571

This study confirms the work have been done by Hussein et al., [25, 26]. The three-dimensional sorting reliabilities algorithm provides an excellent 3-D phase unwrapping, which leads to high quality of 3-D coastline reconstruction. This could be contributed to quality map. Indeed, the 3-DSR algorithm is guided by including the maximum gradient quality maps. Therefore, quality maps guide the unwrapping path through a noisy region so that the interferogram patterns are in completing cycle as compared to InSAR interferogram. Moreover, as stated by Hussien et al., [26], changing the cube size has a great effect to reduce the effect of noise and improve the calculated quality. Consistent with Marghany [42], the 3-DSR algorithm follows discrete unwrapping paths to ensure the processing of the highest quality regions even if they are separated from each other. In other words, within the 3-DSR algorithm, the edges are stored in an array which is based on the terms of the terms of their edge quality values. This means it relies on edge quality to guide the unwrapping path that produces accurate 3-D coastline reconstruction as compared to InSAR techniques. Generally, the 3-DSR algorithm can be an excellent solution for decorrelation problems in such tropical area as Malaysia.

5. Conclusions

The paper has demonstrated InSAR phase unwrapping using the three-dimensional sorting reliabilities algorithm (3-DSR). In addition, three-dimensional (3-D) coastline deformation from interferometry synthetic aperture radar (InSAR) is estimated. Further, three-dimensional sorting reliabilities algorithm (3D-SRA) is implemented with phase unwrapping technique. Consequently, the 3D-SRA is used to eliminate the phase decorrelation impact from the interferograms. The study shows that InSAR produces discontinues interferogram pattern because of the high decorrelation. On the contrary, the three-dimensional sorting reliabilities algorithm generated 3-D coastline deformation with a bias of-0.08 m, lower than ground measurements and the InSAR method. Therefore, the three-dimensional sorting reliabilities algorithm has a standard error of mean of ± 0.05 m, lower than ground measurements and the InSAR method. Consequently, the 3D-SRA is used to eliminate the phase decorrelation impact from the interferograms. The study also shows the performance of InSAR method using the 3D-SRA is better than InSAR procedure which is validated by a lower range of error (0.06±0.32 m) with 90% confidence intervals. In conclusion, the 3-DSR algorithm can be used to solve the problem of decorrelation and produced accurate 3-D coastline deformation using ENVISAT ASAR data.

Author details

Maged Marghany*

Address all correspondence to: maged@utm.my, magedupm@hotmail.com

Institute of Geospatial Science and Technology (INSTeG), University of Technology, Skudai, Johor Bahru, Malaysia

References

[1] Massonnet, D. and Feigl K. L.: Radar interferometry and its application to changes in the earth's surface. *Rev. Geopyh.* 36 (1998) 441--500

[2] Burgmann R. Rosen P.A. and Fielding E.J.: Synthetic aperture radar interferometry to measure Earth's surface topography and its deformation. *Ann. Rev. of Earth and Plan. Sci.* 28: (2000)169--209

[3] Hanssen R.F.: Radar Interferometry: Data Interpretation and Error Analysis, Kluwer Academic, Dordrecht, Boston, (2001)

[4] Zebker H.A., P.A. Rosen, and Hensley S.:Atmospheric effects in inteferometric synthetic aperture radar surface deformation and topographic maps. *J. Geophys. Res.*102 (1997) 7547—7563

[5] Askne J., M. Santoro, G. Smith, and Fransson J. E. S.: Multitemporal repeat-pass SAR interferometry of boreal forests," *IEEE Trans. Geosci. Remote Sens.* 41 (2003) 1540—1550

[6] Nizalapur V., R. Madugundu,and Shekhar Jha C.: Coherence-based land cover classification in forested areas of Chattisgarh, Central India, using environmental satellite-advanced synthetic aperture radar data. *J. Appl. Rem. Sens.* 5 (2011) 059501-1--059501-6

[7] Rao K. S., H. K. Al Jassar, S. Phalke, Y. S. Rao, J. P. Muller, and. Li Z.: A study on the applicability of repeat pass SAR interferometry for generating DEMs over several Indian test sites," *Int. J. Remote Sens.* 27 (2006) 595--616

[8] Rao K. S. and Al Jassar H.K.: Error analysis in the digital elevation model of Kuwait desert derived from repeat pass synthetic aperture radar interferometry. *J. Appl.Remote Sens*.4(2010)1--24

[9] Lee H.: Interferometric Synthetic Aperture Radar Coherence Imagery for Land Surface Change Detection. Ph.D theses, University of London (2001)

[10] Luo X., F.Huang, and Liu G.: Extraction co-seismic Deformation of Bam earthquake with Differential SAR Interferometry. *J. New Zea. Inst. of Surv*. 296 (2006) 20--23

[11] Yang J. T.Xiong and Peng Y.: A fuzzy Approach to Filtering Interferometric SAR Data. *Int. J. of Remote Sens*, 28 (2007) 1375--1382

[12] Gens R. The influence of input parameters on SAR interferometric processing and its implication on the calibration of SAR interferometric data", *Int. J. Remote Sens.* 2 (2000) 11767--1771

[13] Anile A.M., B. Falcidieno, G. Gallo, M. Spagnuolo, Spinello S.: Modeling uncertain data with fuzzy B-splines", Fuzzy Sets and Syst. 113 (2000) 397--410

[14] Marghany M.: Simulation of 3-D Coastal Spit Geomorphology Using Differential Synthetic Aperture Interferometry (DInSAR). In I. Padron.,(ed.) Recent Interferometry Applications in Topography and Astronomy. Croatia: InTech-Open Access Publisher, (2012) 83—94

[15] Spangnolini U.: 2-D phase unwrapping and instantaneous frequency estimation. IEEE Trans.Geo.Remot. Sensing 33:(1995) 579--589

[16] Davidson G. W. and Bamler R. Multiresolution phase unwrapping for SAR interferometry EEE Trans. Geosci. Remote Sensing, 37 (1999) 163--174

[17] Marghany M., Z. Sabu and Hashim M.: Mapping coastal geomorphology changes using synthetic aperture radar data". Int. J. Phys. Sci. 5,(2010)1890—1896

[18] Marghany M.:Three-dimensional visualisation of coastal geomorphology using fuzzy B-spline of dinsar technique. Int. J. of the Phys. Sci. 6 (2011) 6967--6971

[19] ENVISAT, "ENVISAT application [online] Available from http:\www.esa.int [Accessed 2 Febraury 2013].

[20] Zebker H.A.,Werner C.L., P.A. Rosen and Hensley S.: Accuracy of Topographic Maps Derived from ERS-1 Interferometric Radar. *IEEE Geosci. Remote Sens*.2. (1994) 823--836

[21] Baselice F., G. Ferraioli, and Pascazio V.: DEM reconstruction in layover areas from SAR and Auxiliary Input Data IEEE Geosci. Rem. Sensing Letters,6: (2009) 253--257

[22] Ferraiuolo G., V. Pascazio, Schirinzi G. Maximum a Posteriori Estimation of Height Profiles in InSAR Imaging. *IEEE Geosci. Rem. Sensing Letters* (2004) 66--70

[23] Ferraiuolo G., F. Meglio, Pascazio V., and Schirinzi G.: DEM reconstruction accuracy in multichannel SAR interferometry. IEEE Trans. On *Geosci. and Rem.* 47 (2009) 191--201

[24] Ferretti A.,C. Prati, Rocca F.: Multibaseline phase unwrapping for InSAR topography estimation", *Il Nuov Cimento,* 24 (2001) 159--176

[25] Hussein S.A., Gdeist M., Burton D., Lalor M.: Fast three-dimensional phase unwrapping algorithm based on sorting by reliability following a non-continuous path, Optical Measurements System for Industrial Inspection IV conference, Eds Osten, Gorecki and Novak, Proc. SPIE, Vol. 5856-Part 1, (2005) 32--40

[26] Hussein S.A., Munther A., Gdeisat, David R.,Burton, Michael J., Lalor, F.Lilley, and Moore C.: Fast and roubust three-diemsional best bath phase unwrapping algorithm. Appl. Opt., 46: (2007) 6623--6635.

[27] Marghany M.: DInSAR technique for three-dimensional coastal spit simulation from radarsat-1 fine mode data. Acta Geophy. 61:(2013) 478--493

[28] Marghany M.: Three dimensional Coastal geomorphology deformation modelling using differential synthetic aperture interferometry. Verlag Der Zeitschrift fur Naturforschung. 67a: (2012) 419--420.

[29] Marghany M.: DEM reconstruction of coastal geomorphology from DInSAR. In Murgante B. et al. (eds): Lecture Notes in Computer Science (ICCSA 2012), Part III, LNCS 7335: (2012) 435--446

[30] Marghany M.: Intermonsoon water mass characteristics along coastal waters off Kuala Terengganu, Malaysia. Int.J.of Phys. Sci 7:(2012) 1294--1299

[31] Marghany M.: Modelling shoreline rate of changes using holographic interferometry. Int.J.of Phys. Sci. 6: (2011) 7694—7698

[32] Wei X and Cumming I. A Region-Growing Algorithm for InSAR Phase Unwrapping.IEEE Trans. On GRS, 1999, 37(1): 124-134

[33] M. Costantini. A Novel Phase Unwrapping Method based on Network Programming. IEEE Trans. On GRS, 1998, 36(3): 813-831.

[34] Goldstein R M, Zebker H A, andWerner C L.Satellite radar interferometry : twodimensional phase unwrapping. Radio Sci., 1988,23(4):713-720.

[35] Ireneusz B,Stewart M P, Kampes P M, Zbigniew P, and Peter L. A Modification to the Goldstein Radar Interferogram Filter. IEEE Trans. On GRS, 2003, 41(9):2114-2118.

[36] Nan W, Da-Zheng F, and Junxia L. A locally adaptive filter of interferometric phase images. IEEE GRS Letters, 2006, 3(1):73-77.

[37] Qifeng Yu, Xia Yang, Sihua Fu, Xiaolin Liu, and Xiangyi Sun. An Adaptive Contoured Window Filter for Interferometric Synthetic Aperture Radar. IEEE GRS Letters, 2007, 4(1):23-26.

[38] Marghany M. Simulation of 3-D Coastal Spit Geomorphology Using Differential Synthetic Aperture Interferometry (DInSAR). In Padron I. (ed.) "Recent Interferometry Applications in Topography and Astronomy". InTech-Open Access Publisher, University Campus STeP Ri, Croatia. (2012),83-94.

[39] Marghany M. Simulation of three dimensional of coastal erosion using differential interferometry synthetic aperture radar. Global nest Journal (2014), 16(1): 80-86.

[40] Pepe A. Advanced Multitemporal Phase Unwrapping Techniques for DInSAR Analyses. In Padron I. (ed.) "Recent Interferometry Applications in Topography and Astronomy". InTech-Open Access Publisher, University Campus STeP Ri, Croatia. (2012),57-82.

[41] Hai L and Renbiao W. Robust Interferometric Phase Estimation in InSAR via Joint Subspace Projection. Hai Li and Renbiao Wu (2012) Robust Interferometric Phase Estimation in InSAR via Joint Subspace Projection. In Padron I. (ed.) "Recent Interfer-

ometry Applications in Topography and Astronomy". InTech-Open Access Publisher, University Campus STeP Ri, Croatia. (2012), 111-132.

[42] Marghany. Three Dimensional Coastline Deformation from Insar Envisat Satellite Data. In Beniamino Murgante, Sanjay Misra, Maurizio Carlini, Carmelo M. Torre, Hong-Quang Nguyen, David Taniar, Bernady O. Apduhan, and Osvaldo Gervasi Computational Science and Its Applications – ICCSA 2013, 2013, (7972) 599-610.

IntechOpen

IntechOpen